

FIG. 1. Calculated loss vs GaAs cap layer thickness (n -DBR=32 pairs; p -DBR=23.5 pairs).

higher loss can be introduced only to the interelement regions (Ti regions).

In our studies, the built-in index step and array pattern are achieved by a selective etching process and two-step metalorganic chemical vapor deposition growth.¹² The element regions (6 μm wide with a 5 μm wide metal opening) include 32 pairs of AlAs/GaAs n -distributed Bragg reflector (DBR), a $1\text{-}\lambda$ optical cavity, which consists of three InGaAs quantum wells, GaAs barrier layers, and $\text{Al}_{0.3}\text{Ga}_{0.70}\text{As}$ confinement layers for 980 nm emission, and 23.5 pairs of $\text{Al}_{0.15}\text{Ga}_{0.85}\text{As}/\text{AlAs}$ p -DBRs. The interelement regions are formed by adding two thin spacer layers of GaAs and GaInP above the fourth pair of $\text{Al}_{0.15}\text{Ga}_{0.85}\text{As}/\text{AlAs}$ p -DBR. According to effective index theory, for a VCSEL,¹³ a lateral effective index step Δn for antiguiding forms due to redshifting of the optical resonance within the interelement regions. The interelement spacing, s , is varied so as to select either in-phase or out-of-phase array mode. Based on the 1D loss calculation, three different GaAs cap thicknesses, t_{cap} in Fig. 1 have been chosen; 45, 57, and 70 nm ($1/4$ wave thickness). Both rectangular (four nearest neighbor) and triangular (six nearest neighbor) array configurations have been fabricated and studied.

Pulsed (100 ns, 1% duty cycle) far-field measurements from both rectangular and triangular array configurations are performed. Near-diffraction-limited-beam, in-phase mode emission, in excellent agreement with the calculated far-field patterns, has been found in array structures as large as 10×10 (100 elements) with $t_{\text{cap}}=0.045$ or $0.057 \mu\text{m}$. Lasing occurs primarily in either the in-phase mode or out-of-phase mode, depending on the particular value of interelement spacing, although some devices have shown a mixture of both in-phase and out-of-phase mode or intermediate mode operation. In array structures with $t_{\text{cap}}=0.070 \mu\text{m}$, most of the devices exhibit a complex mixture of in-phase, out-of-phase, intermediate mode. The measured far-field scans (horizontal and vertical) of a 10×10 rectangular array with $t_{\text{cap}}=0.045 \mu\text{m}$ are shown in Fig. 2(b). The corresponding calculated far-field pattern is also shown in Fig. 2(a) for comparison. The measured center beam width is about 0.58° , which is close to the value estimated for the diffraction limit (DL) based on the total size of the aperture. Larger 20×20 array structures also operate primarily in phase, however, the beam width is three to four times the diffraction limit. The measured $P-I$ (1 μs , 1% duty cycle) and corresponding far-

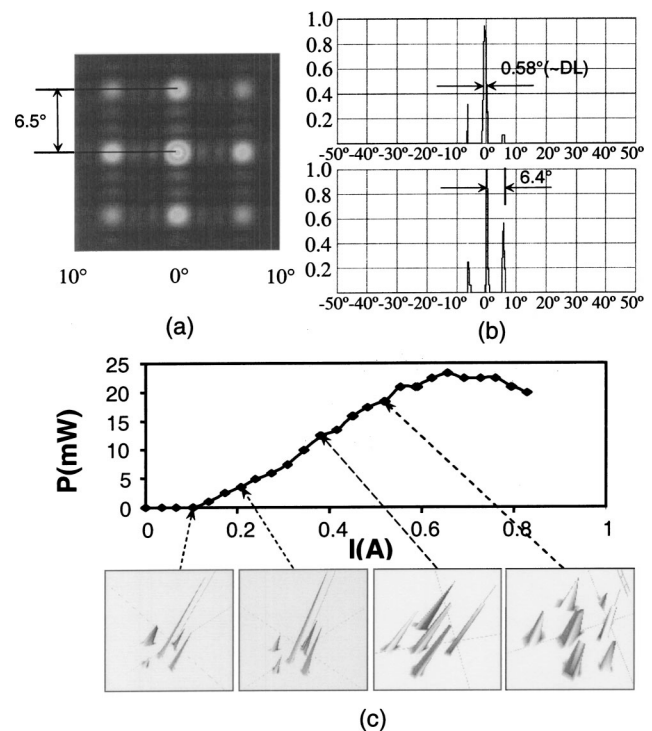


FIG. 2. (a) Calculated in-phase mode far field, (b) measured 1D cross section of far field (top: vertical, bottom: horizontal) in a 10×10 rectangular array (interelement width, $s=3.0 \mu\text{m}$), (c) measured in-phase mode far field and power output vs the pulsed driving current (pulse width=2 μs) in a 10×10 rectangular array ($s=3.0 \mu\text{m}$)

field interference patterns at various drive levels for the same device are shown in Fig. 2(c). From this, we can see that this device maintains a relatively stable far-field pattern with driving current up to $>5 \times I_{\text{th}}$, indicating that the in-phase mode dominates over a large current range. Nevertheless, broadening of the center lobe at high drive currents indicates the onset of additional (intermediate) array modes. The relatively low external differential efficiency ($\sim 3\%$) is believed to result from an unoptimized p -DBR pair number and large aperture array heating for the 1 μs pulse width utilized. To minimize heating, a junction-down configuration is preferred.

Triangular arrays have also been found to exhibit in-phase mode operation. The measured far-field profile and corresponding calculated profile for a 19 element triangular array are shown separately in Figs. 3(b) and 3(a), respectively. The measured center beam width, 1.41° , is about 1.16 times the estimated diffraction limit based on the total aperture size. A three-dimensional (3D) view of the measured far-field pattern with driving current up to 200 mA (about $4 \times I_{\text{th}}$) is depicted in Fig. 3(c). We find the triangular arrays have an improved ability to maintain a stable in-phase mode pattern with an increase in drive current compared to rectangular arrays. We believe this is due to stronger element coupling in triangular arrays (more nearest neighbors), although detailed studies are still necessary. In addition, certain competing adjacent modes present in rectangular arrays, like the one with an even number of intensity peaks in one direction and an odd number of intensity peaks in the other direction, are no longer supported by the triangular array geometry.

The influence of interelement spacing on array modal behavior has also been studied. Devices which exhibit in-

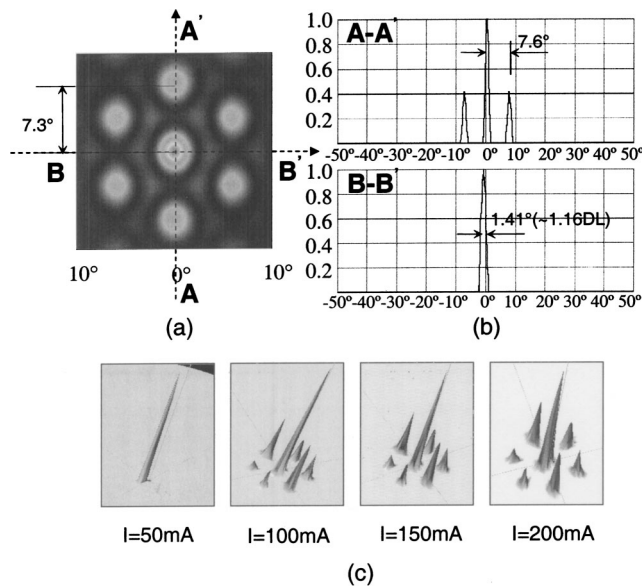


FIG. 3. (a) Calculated in-phase mode far field, (b) measured 1D cross section of far field (top: vertical, bottom: horizontal) in a 19 element triangular array (interelement width, $s = 2.0 \mu\text{m}$), (c) measured in-phase mode far field vs the pulsed driving current (pulse width = 2 100 ns) in a 19 element triangular array (interelement width, $s = 2.0 \mu\text{m}$)

phase mode and out-of-phase mode as a function of interelement spacing, s , are summarized in Fig. 4. For rectangular arrays, the in-phase mode is favored around $s = 3.0 \mu\text{m}$, whereas the out-of-phase mode is favored around $s = 1.5\text{--}2.0 \mu\text{m}$. For triangular arrays, in-phase mode is favored around $s = 3.5 \mu\text{m}$ and out-of-phase mode is favored around $s = 1.5 \mu\text{m}$. The 1D lateral leaky-wave resonance condition can be calculated from the index step and interelement width s .¹⁰ From a 1D transfer matrix calculation, the index step is estimated to be $\Delta n = 0.015$, resulting in a lateral leaky-wave wavelength of $2.98 \mu\text{m}$. Therefore, the lateral resonance condition is satisfied for s values around $1.5 \mu\text{m}$ (for in-phase-mode) or $3 \mu\text{m}$ (for out-of-phase mode). As expected from theory, the out-of-phase mode is generally favored at the in-phase mode resonance position, $s \sim 1.5 \mu\text{m}$, because of lower edge radiation loss for the non-resonant out-of-phase mode. Similarly, the in-phase mode is favored at the out-of-phase resonance position $s \sim 3.0 \mu\text{m}$. Simulations studies using a 3D bidirectional beam propagation model¹² are in good agreement with the measurements. These simulations also indicated that improved modal discrimination can be achieved by increasing the amount of loss in the interelement regions, thereby allowing the resonant mode to have the lowest threshold gain.

In conclusion, we have demonstrated near-diffraction-limited in-phase mode coherent emission from very large aperture (up to 100 elements) antiguided VCSEL arrays. Both rectangular and triangular antiguided VCSEL have demonstrated primarily in-phase mode operation with a relatively stable far-field pattern with an increase in drive current. Improved modal discrimination is expected to be real-

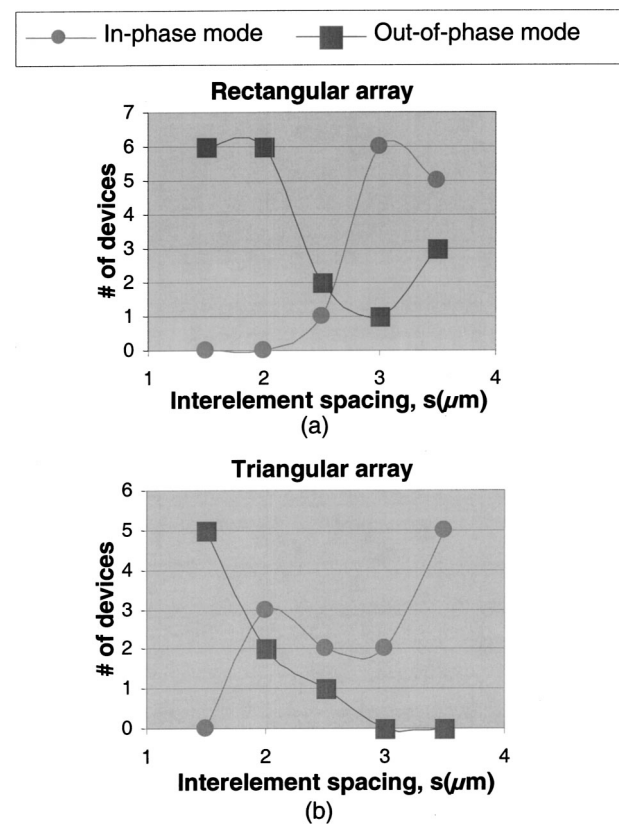


FIG. 4. Number of devices vs interelement spacing, s (μm), for in-phase mode and out-of-phase mode. (a) Rectangular arrays. (b) Triangular arrays.

ized by incorporating increased interelement loss. Structure optimization and a suitable thermal package design are also needed to further increase output power in these large aperture array devices.

This work was supported by NSF Project No. 0139823. The authors at TRINITI also acknowledge partial support by Russian Foundation for Basic Research Project No. 02-02-17101.

- ¹L. J. Mawst, IEEE Circuits Devices Mag. **19**, 34 (2003).
- ²Kuo-Liang Chen and Shyh Wang, Appl. Phys. Lett. **47**, 555 (1985).
- ³F. Monti di Sopra, M. Brunner, H.-P. Gauggel, H. P. Zappe, M. Moser, R. Hover, and E. Kapon, Appl. Phys. Lett. **77**, 2283 (2000).
- ⁴P. L. Gourley, M. E. Warren, G. R. Hadley, G. A. Vawter, T. M. Brennan, and B. E. Hammons, Appl. Phys. Lett. **58**, 890 (1991).
- ⁵G. R. Hadley, Opt. Lett. **15**, 1215 (1990).
- ⁶M. E. Warren, P. L. Gourley, G. A. Vawter, T. M. Brennan, B. E. Hammons, and K. L. Lear, Appl. Phys. Lett. **61**, 1484 (1992).
- ⁷D. Botez, M. Jansen, L. J. Mawst, G. Peterson, and T. J. Roth, Appl. Phys. Lett. **58**, 2070 (1991).
- ⁸D. K. Serkland, K. D. Choquette, G. R. Hadley, K. M. Geib, and A. A. Allerman, Appl. Phys. Lett. **75**, 3754 (1999).
- ⁹D. Zhou and L. J. Mawst, Appl. Phys. Lett. **77**, 2307 (2000).
- ¹⁰D. Zhou, L. J. Mawst, and Z. Dai, IEEE J. Quantum Electron. **38**, 652 (2002).
- ¹¹D. Botez, L. J. Mawst, G. L. Peterson, and T. J. Roth, IEEE J. Quantum Electron. **26**, 482 (1990).
- ¹²N. N. Elkin, A. P. Napartovich, D. V. Vysotsky, V. N. Troshchieva, L. Bao, N. Kim, D. Zhou, and L. J. Mawst, Proc. SPIE **4994**, 112 (2003).
- ¹³G. R. Hadley, Opt. Lett. **20**, 1483 (1995).